

## COMMUNICATION

## Virus-mimicking nano-constructs as a contrast agent for near infrared photoacoustic imaging†‡

Cite this: *Nanoscale*, 2013, 5, 1772Sharad Gupta,<sup>§a</sup> Muhammad R. Chatni,<sup>§b</sup> Ayala L. N. Rao,<sup>c</sup> Valentine I. Vullev,<sup>a</sup> Lihong V. Wang<sup>\*b</sup> and Bahman Anvari<sup>\*a</sup>

Received 16th December 2012

Accepted 4th January 2013

DOI: 10.1039/c3nr34124k

[www.rsc.org/nanoscale](http://www.rsc.org/nanoscale)

We report the first proof-of-principle demonstration of photoacoustic imaging using a contrast agent composed of a plant virus protein shell, which encapsulates indocyanine green (ICG), the only FDA-approved near infrared chromophore. These nano-constructs can provide higher photoacoustic signals than blood in tissue phantoms, and display superior photostability compared to non-encapsulated ICG. Our preliminary results suggest that the constructs do not elicit an acute immunogenic response in healthy mice.

In this communication, we report the first demonstration of near infrared (NIR) photoacoustic imaging (PAI) using a new nano-construct composed of biological and organic materials as the contrast agent. Specifically, the construct is comprised of a protein shell, purified from the plant-infecting brome mosaic virus (BMV), that encapsulates indocyanine green (ICG), the only FDA-approved NIR chromophore. We refer to these virus-resembling nano-constructs as optical viral ghosts (OVGs) since the genomic content of the wildtype BMV is eliminated and replaced with ICG, while the capsid protein (CP) subunits remain as the encapsulating shell.

Recently, attention has been given to the use of biological materials, particularly viruses, as a platform for the delivery of imaging and therapeutic agents.<sup>1–5</sup> Plant and recombinant adenoviruses have been investigated as potential vaccine carriers in gene therapy and oncolytic viral therapy.<sup>6–8</sup> Viruses have also been used to encapsulate inorganic materials

including quantum dots (QDs),<sup>9</sup> gold,<sup>10</sup> and magnetic nanoparticles.<sup>11</sup> Virus-based protein cages, assembled from the cowpea chlorotic mottle virus,<sup>12</sup> and the capsid of the MS2 bacteriophage coated with gadolinium have been investigated as MRI contrast agents.<sup>12,13</sup>

In comparison to animal viruses, plant viruses are easier to produce and purify, and are chemically and structurally more stable.<sup>5,14,15</sup> For example, surface conjugation of the cowpea mosaic virus (CPMV) with a folic acid-PEG moiety has been demonstrated *in vitro* to allow specific recognition of tumor cells bearing the folate receptor.<sup>16</sup> The potato virus X surface-labeled with Oregon Green 488 and Alexa Fluor 647 has been successfully used to image mouse fibroblasts and human cervical cancer cells *in vitro*.<sup>17</sup> Recently, the surface of RNA containing CPMV was labeled with Alexa Fluor 555, a non-NIR fluorophore, and used for *in vivo* vascular imaging in mice and chick embryos.<sup>18</sup> Results of this study are extremely encouraging, in that they demonstrate the potential of using a fluorescently labeled plant virus for successful *in vivo* vascular imaging. In another recent study, fluorescence imaging of human prostate tumor xenografts on the chicken chorioallantoic membrane animal model was achieved by using CPMV decorated with NIR Alexa Fluor 647, and functionalized with peptide bombesin to target gastrin-releasing peptide receptors.<sup>19</sup> An engineered variant of CPMV has also been used as a template for fabrication of silica nanoparticles.<sup>20</sup>

We recently provided the first report of successful fabrication of the genome-depleted BMV virions doped with ICG, and their utility in fluorescence imaging.<sup>21</sup> ICG (molecular weight of its sodium salt,  $\text{MW}(\text{C}_{43}\text{H}_{47}\text{N}_2\text{NaO}_6\text{S}_2) \approx 775$  Da) is an excellent NIR light absorber with reported values of its molar extinction coefficient ( $\epsilon$ ) in aqueous media ranging between  $8 \times 10^4$  and  $1.2 \times 10^5$   $\text{l mol}^{-1} \text{cm}^{-1}$  at 780 nm, which corresponds to absorption cross-section,  $\sigma_a$  (780 nm), of about  $3 \times 10^{-16}$  to  $4.6 \times 10^{-16}$   $\text{cm}^2$ .<sup>22–24</sup> Therefore, the strong absorption properties of ICG can be explored as an alternative to radiative-based (*e.g.*, fluorescence) imaging modalities. Photoacoustic (PA) techniques offer such an absorption-mediated imaging approach.

<sup>a</sup>Department of Bioengineering, University of California, Riverside, Riverside, CA 92521, USA. E-mail: [anvarib@ucr.edu](mailto:anvarib@ucr.edu)

<sup>b</sup>Department of Biomedical Engineering, Washington University in St. Louis, St. Louis, MO 663130, USA. E-mail: [lhwang@seas.wustl.edu](mailto:lhwang@seas.wustl.edu)

<sup>c</sup>Department of Plant Pathology and Microbiology, University of California, Riverside, Riverside, CA 92521, USA

† Authors have no competing financial interest.

‡ Electronic supplemental information (ESI) available: Information on experimental procedure for fabrication of the nano-constructs, photoacoustic imaging, and immunogenic studies. See DOI: 10.1039/c3nr34124k

§ These authors contributed equally to this work.

In PAI, light is absorbed, and converted into heat. Depending on the radiant exposure levels, temperature rises on the order of  $\approx 1$  °C is sufficient to produce acoustic waves, which are then detected by ultrasound detector(s).<sup>25,26</sup> The PA approach keeps the merits of optical imaging techniques, such as optical sensitivity and radiation safety, while providing high ultrasound-defined spatial resolution in optical quasi-diffusive and diffusive regimes. As an endogenous contrast agent for PAI, hemoglobin has been investigated in several applications such as visualizing brain structure and lesions,<sup>25,27</sup> delineating tumor vasculature,<sup>28</sup> monitoring hemodynamics,<sup>29</sup> imaging small animals,<sup>30</sup> and measuring blood flow in microvasculature.<sup>31</sup> One of the key properties of tumor growth is neo-angiogenesis, and the PA approach has been used to detect tumor growth by imaging the hemoglobin in such vasculatures. Melanin, as another endogenous PA contrast agent, has been used for the diagnosis, prognosis, and treatment planning of melanotic melanoma.<sup>32,33</sup>

We present a transmission electron microscope (TEM) image of OVGs after 15 days of storage in BMV suspension buffer (Fig. 1A), confirming that the OVGs remained intact in the suspension buffer over this time interval. From the recorded TEM images, we assessed the size and the monodispersity of the OVGs. The image analysis yielded a diameter of  $29.7 \pm 3.1$  nm, where the error limit of the mean represents one standard deviation. We have previously employed dynamic light scattering (DLS) to estimate the size of ICG-doped viral construct, similar to the OVGs used in this study, *i.e.*, BMV CP to ICG concentration ratio of 4, and ICG concentration of  $\sim 30$   $\mu\text{M}$ .<sup>21</sup> Our DLS analysis yielded OVG diameter of  $24.3 \pm 3.9$  nm,<sup>21</sup> which was in a good agreement with our TEM results.

We present an illustrative absorption spectrum of OVGs in BMV suspension buffer (Fig. 1B). This set of OVGs was fabricated using  $20 \mu\text{g ml}^{-1}$  of ICG ( $\approx 26 \mu\text{M}$ ), and the final solution containing the OVGs was diluted by a factor of 10. The ratio of BMV CP to ICG concentration was fixed at 4 in fabricating the OVGs used in this study. The OVG absorption spectrum displays maximum absorbance peaks at  $\approx 700$  and  $800$  nm. The peak at 270 nm corresponds to absorption by the CP subunits encapsulating ICG, consistent with our previous report.<sup>21</sup> The spectrum of the OVG supernatant solution, measured after OVG

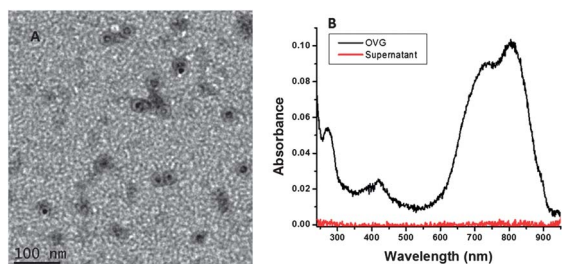


**Fig. 1** Physical characterization of OVGs. (A) TEM image of OVGs obtained after 15 days of storing the OVGs in BMV suspension buffer. (B) Absorption spectrum of OVGs (black trace) corresponding to constructs fabricated using ICG concentration of  $20 \mu\text{g ml}^{-1}$  ( $\approx 26 \mu\text{M}$ ). The final solution containing the OVGs was subsequently diluted ten times prior to obtaining the spectrum. The red trace in panel B corresponds to the spectrum of the supernatant solution.

fabrication, did not display any absorbance over the entire UV-NIR spectral band, confirming that almost all the ICG introduced during the fabrication process was incorporated into the constructs (*i.e.*,  $\approx 100\%$  loading efficiency), and that the entire CP subunits were utilized in forming the OVGs.

We present the averaged B-scan of tubes containing various samples embedded at and below the surface of chicken breast tissue as a phantom (Fig. 2). The designation of samples is as follows: sample 10S represents OVGs prepared using  $10 \mu\text{g ml}^{-1}$  of ICG ( $\approx 13 \mu\text{M}$ ) during fabrication; 20S is the OVG sample constructed using  $20 \mu\text{g ml}^{-1}$  of ICG ( $\approx 26 \mu\text{M}$ ); 40S is the OVG sample constructed using  $40 \mu\text{g ml}^{-1}$  of ICG ( $\approx 52 \mu\text{M}$ ); 20S/4 is the 20S sample diluted by factor of four; and 40S/4 and 40S/10 are the 40S samples diluted by factors of 4 and 10, respectively. The near and far walls of all the tubes are visible. The mean amplitude of the PA signal at the top surface of the tubes was determined and plotted as a function of excitation wavelength.

Regardless of the placement positions of the tubes within the chicken breast phantom, the tubes containing the 40S OVG solution gave the highest PA signal since they had the highest concentration of ICG loaded into the OVG constructs. The amplitude of the PA signal emitted from the tube containing the 40S OVG solution was about 3–4 times higher than that of blood independent of the tubes depth in the phantom. The 20S OVG solution had two-fold higher PA signal than blood with tubes placed at the surface (Fig. 2A) or 6 mm subsurface (Fig. 2B).

The PA signals from diluted 20S/4 and 40S/10 OVG solutions were similar in magnitude, but lower than that of blood in response to excitation wavelengths longer than 770 nm regardless of the placement depth of the tubes. Independent of

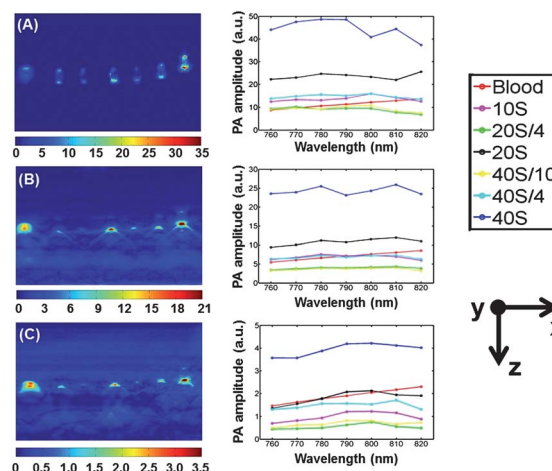


**Fig. 2** Averaged B-scan photoacoustic images in response to 790 nm excitation (left panel) and the corresponding PA signal amplitudes as a function of excitation wavelength (right panel). Photoacoustic images correspond to tubes containing the OVG samples and oxygenated blood in *ex vivo* chicken tissue phantoms: (A) no overlaid chicken tissue, (B)  $\approx 6$  mm overlaid chicken tissue, and (C)  $\approx 14$  mm overlaid chicken tissue. Left to right in B-scan images: Oxygenated blood, 10S, 20S/4, 20S, 40S/10, 40S/4, and 40S OVG solutions. The designation of samples is as follows: sample 10S represents OVGs prepared using  $10 \mu\text{g ml}^{-1}$  ( $\approx 13 \mu\text{M}$ ) of ICG during fabrication; 20S is the OVG sample constructed using  $20 \mu\text{g ml}^{-1}$  of ICG; 40S is the OVG sample constructed using  $40 \mu\text{g ml}^{-1}$  of ICG; 20S/4 is the 20S sample diluted by factor of four; and 40S/4 and 40S/10 are the 40S samples diluted by factors of 4 and 10, respectively.

the tubes depth in the phantom, the PA signal from blood increased approximately by 50% when changing the excitation wavelength from 760 nm to 820 nm, which is consistent with absorption of oxygenated blood in that wavelength range.

When tubes were placed 6 mm below the surface of the phantom, there was a reduction in the PA signal from the 10S and 40S/4 OVG samples (Fig. 2C). This reduction could be due to the non-uniformity in the optical properties across the whole tissue, resulting in higher attenuation of the laser light at some part of the tissue.

To investigate the feasibility of deeper imaging,  $\approx 14$  mm thick chicken breast tissue was overlaid on top of the seven tubes. The PA signal from the 40S OVG solution remained the highest, and approximately three times higher than that of blood (Fig. 2C). The PA signal from the 20S OVG solution was similar to that of blood across the entire wavelength range.

The PA signals for both OVG (20S) and free ICG ( $20 \mu\text{g ml}^{-1}$ ) in BMV suspension buffer solutions decreased with increasing number of laser pulses (Fig. 3). However, the PA signal associated with free ICG solution was lower than that associated with the OVG solution for all laser number pulses investigated, and this difference increased with increasing number of the laser pulse. For example, the PA signal from the OVG solution was reduced by  $\approx 20\%$  from its maximum intensity, whereas the signal from the ICG solution decreased by  $\approx 45\%$ , both after 50 laser pulses.

While the safety of OVGs needs to be established based on future *in vivo* studies, our previous *in vitro* results indicate that mammalian cells remain viable following internalization of these constructs.<sup>21</sup> To our knowledge, there is no prior application of plant viruses, or constructs derived from plant viruses in humans. Herein, we report the first results to assess the immunogenic effects of the BMV CP in mice (Fig. 4). We administered purified BMV CP subunits ( $100 \mu\text{g}$ ) into healthy mice through tail vein injection. As positive control, we administered  $\approx 80 \mu\text{g}$  of lipopolysaccharide (LPS) ( $80 \mu\text{l}$  injection volume), a known immunogenic agent.<sup>34</sup> Following euthanasia at one or six hours post-injection, we screened for the production of interleukin-6 (IL-6), tumor necrosis factor- $\alpha$

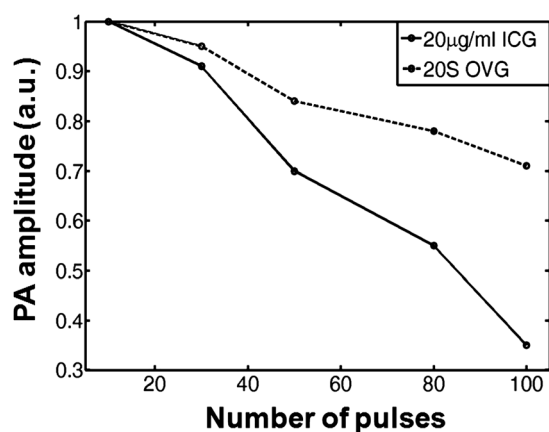


Fig. 3 Photoacoustic amplitude response of OVGs (upper trace) and non-encapsulated ICG (lower trace) as a function of applied laser pulses.

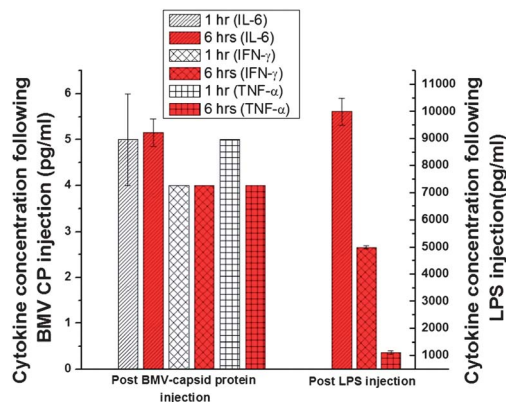


Fig. 4 Cytokine levels in healthy mice injected with purified BMV CP, or LPS (positive control). Each bar represents the mean  $\pm$  standard deviation values from three wells (some of the errors bars were too small to be shown).

(TNF $\alpha$ ), and interferon- $\gamma$  (IFN $\gamma$ ) cytokines. IL-6 and TNF $\alpha$  are among inflammation-associated cytokines, secreted by macrophages and other cell types. They stimulate the production of specific plasma proteins during the acute phase following an inflammatory stimulus.<sup>35</sup> IFN $\gamma$  is a cytokine critical for innate and adaptive immunity against viral and intracellular pathogens, and tumor control.<sup>36</sup>

In response to injection of the BMV CP subunits, very low levels of the cytokines IL-6, TNF $\alpha$ , and IFN $\gamma$  ( $<6 \text{ pg ml}^{-1}$ ) were measured. However, administration of LPS resulted in production of approximately  $1,100 \text{ pg ml}^{-1}$  of TNF $\alpha$ ,  $5000 \text{ pg ml}^{-1}$  of IFN $\gamma$ , and  $10,000 \text{ pg ml}^{-1}$  of IL-6 at six hours post-injection. Although further dose-response and multiple injection studies must be performed, these preliminary results suggest that OVGs may not elicit an inflammatory response.

In a recent study, the toxicity of the CPMV was investigated in mice.<sup>37</sup> Histological examinations of various organs revealed no pathological changes. Specific detection of apoptotic cells in liver, spleen, lung, kidneys, and heart was not observed. In another study, the biodistribution of cowpea protein cages was investigated in mice.<sup>38</sup> There was  $\approx 65\%$  elimination of protein cages through the urine and feces at 24 hours post tail vein injection of naive and immunized mice. The investigators reported no overt toxicity after a single injection, and indicated that protein cages may serve as safe, biocompatible, nano-platforms for applications in medicine.

While ICG has been used clinically as a fluorescence imaging probe in retinal angiography as well as cardiovascular and liver function assessment,<sup>39–41</sup> its main drawbacks are its rapid clearance from the vasculature with nearly exclusive uptake by hepatocytes, and immense propensity for aggregation resulting in fluorescence quenching. Specifically, after intravascular administration, ICG readily binds to albumin and high-density lipoproteins such as alpha-1 lipoprotein,<sup>42</sup> and is eliminated from circulation with plasma clearance half-life on the order of 3–4 minutes.<sup>43,44</sup> Encapsulation of ICG can provide a method to shield the ICG from non-specific interactions with plasma proteins, and increase its lifetime within plasma. Saxena *et al.* have reported that ICG encapsulation into poly

(DL-lactic-co-glycolic acid) (PLGA) constructs resulted in nearly six times higher ICG levels within the plasma at one hour post tail vein injection in mice, as compared to non-encapsulated ICG.<sup>45</sup> At four hours post-injection, there was still detectable ICG within the plasma when administered in nano-encapsulated formulation.<sup>45</sup> Our group has previously reported that encapsulation of ICG into polymeric nano-constructs, composed of poly(allylamine) hydrochloride cross-linked with disodium biphosphate, enhances the contrast of *in vivo* fluorescent images from heart and lungs for at least up to 90 minutes after tail vein injection in mice,<sup>46</sup> indicating the prolonged circulation of ICG when encapsulated. While future studies are required, encapsulation of ICG into virus-based constructs, such as the OVGs, may provide a method for prolonged PAI as compared to PAI in conjunction with non-encapsulated ICG.

Our results demonstrate that encapsulation in the OVG constructs improves the photostability of ICG (Fig. 3). The observed loss of the NIR absorption of free ICG upon irradiation can be ascribed to photo-induced breaking of the  $\pi$ -conjugation along the *oligo*-methine linker between the two aromatic moieties in the dye molecule. Therefore, photo-addition to the altering double bonds (producing a leuco form of the dye with converted  $sp^2$  to  $sp^3$  carbon hybridization) and/or photocleavage of the *oligo*-methine linker can account for the observed decrease in the NIR absorption and emission of free ICG.<sup>47,48</sup> Holzer *et al.* showed that placing ICG in an aprotic organic solvent leads to more than about two orders of magnitude decrease in the time-zero degradation yield ( $\phi_{D,0}$ ) of the dye in comparison with  $\phi_{D,0}$  for aqueous solutions.<sup>48</sup> Similar effect was observed when ICG was dissolved in human plasma where the dye can bind to the abundant human serum albumin and other proteins.<sup>48</sup> Although the exact chemical mechanism of ICG photo-degradation is not known, these reported evidence indicate that the removal of nucleophiles, such as water molecules, from the microenvironment of the cyanine dye, considerably improves its photostability. Our findings are consistent with this previous evidence. Encapsulation of ICG within the constructs limits the access of water to the dye molecules, resulting in the observed improvement in the ICG photostability.

OVGs may provide a versatile platform for development of a multi-functional nano-construct with potential for site-specific, and combined deep tissue optical imaging and phototherapy. The abundance of naturally present amines on the CP shell provides addressable sites for covalent attachment of a variety of targeting moieties on the surface of OVGs so that the constructs can be used to identify molecular biomarkers of a disease. As an example, in a recent study, we functionalized the surface of OVGs with the anti-epidermal growth factor receptor, and subsequently utilized these constructs for targeted fluorescence imaging of human bronchial epithelial cancer cells *in vitro*.<sup>49</sup> Such functionalized OVGs may potentially be used in conjunction with PAI for targeted imaging at high optical contrast. Fabrication and functionalization procedures are relatively inexpensive, and easily achieved at room temperature and pressure without the need for any chemical synthesis procedures.

## Conclusions

We report the first proof-of-principle demonstration of NIR-PAI using virus-mimicking particles. When used at appropriate amounts, OVGs displayed a much stronger photoacoustic signal than that emitted by blood over the wavelength range of 760–820 nm. OVGs also demonstrated superior photostability in comparison to non-encapsulated ICG in solution. Our preliminary results showed that OVGs did not elicit an acute immunogenic response in healthy mice.

## Acknowledgements

This work was sponsored in part by grants from the National Science Foundation (CBET-1144237, CBET-0923408 and CBET 0935995), and National Institutes of Health (R01-EB000712, R01-EB008085, R01-CA134539, U54-CA136398, R01-CA157277, and R01-CA159959). To create the color graphic, we modified some of the images freely available from the RCSB PDB (<http://www.pdb.org>) of PDB 1BNA (H. R. Drew, R. M. Wing, T. Takano, C. Broka, S. Tanaka, K. Itakura and R. E. Dickerson, *Proc. Natl. Acad. Sci. U. S. A.*, 1981, **78**, 2179–2183). We thank Mr Yadir Guerrero for his contribution towards creating the color graphic.

## References

- 1 Y. Liu, Y. Fang, Y. Zhou, E. Zandi, C. L. Lee, K. I. Joo and C. P. Wang, *Small*, 2012, DOI: 10.1002/sml.201201661.
- 2 I. Yildiz, S. Shukla and N. F. Steinmetz, *Curr. Opin. Biotechnol.*, 2011, **22**, 901–908.
- 3 M. Manchester and P. Singh, *Adv. Drug Delivery Rev.*, 2006, **58**, 1505–1522.
- 4 R. Singh and K. Kostarelos, *Trends Biotechnol.*, 2009, **27**, 220–229.
- 5 M. Young, D. Willits, M. Uchida and T. Douglas, *Annu. Rev. Phytopathol.*, 2008, **46**, 361–384.
- 6 F. R. Brennan, T. D. Jones and W. D. Hamilton, *Mol. Biotechnol.*, 2001, **17**, 15–26.
- 7 T. Tanaka, M. Kuroki, H. Hamada, K. Kato, T. Kinugasa, H. Shibaguchi, J. Zhao and M. Kuroki, *Anticancer Res.*, 2007, **27**, 3679–3684.
- 8 Z. S. Guo, S. H. Thorne and D. L. Bartlett, *Biochim. Biophys. Acta*, 2008, **1785**, 217–231.
- 9 S. K. Dixit, N. L. Goicochea, M. C. Daniel, A. Murali, L. Bronstein, M. De, B. Stein, V. M. Rotello, C. C. Kao and B. Dragnea, *Nano Lett.*, 2006, **6**, 1993–1999.
- 10 N. L. Goicochea, M. De, V. M. Rotello, S. Mukhopadhyay and B. Dragnea, *Nano Lett.*, 2007, **7**, 2281–2290.
- 11 X. L. Huang, L. M. Bronstein, J. Retrum, C. Dufort, I. Tsvetkova, S. Aniyagei, B. Stein, G. Stucky, B. McKenna, N. Remmes, D. Baxter, C. C. Kao and B. Dragnea, *Nano Lett.*, 2007, **7**, 2407–2416.
- 12 M. Allen, J. W. M. Bulte, L. Liepold, G. Basu, H. A. Zywicke, J. A. Frank, M. Young and T. Douglas, *Magn. Reson. Med.*, 2005, **54**, 807–812.

- 13 E. A. Anderson, S. Issacman, D. S. Peabody, E. Y. Wang, J. W. Canary and K. Kirshenbaum, *Nano Lett.*, 2006, **6**, 1160–1164.
- 14 K. J. Koudelka, G. Destito, E. M. Plummer, S. A. Trauger, G. Siuzdak and M. Manchester, *PLoS Pathog.*, 2009, **5**, e1000417.
- 15 L. Lavelle, J. P. Michel and M. Gingery, *J. Virol. Methods*, 2007, **146**, 311–316.
- 16 G. Destito, R. Yeh, C. S. Rae, M. G. Finn and M. Manchester, *Chem. Biol.*, 2007, **14**, 1152–1162.
- 17 N. F. Steinmetz, M. E. Mertens, R. E. Taurog, J. E. Johnson, U. Commandeur, R. Fischer and M. Manchester, *Nano Lett.*, 2010, **10**, 305–312.
- 18 J. D. Lewis, G. Destito, A. Zijlstra, M. J. Gonzalez, J. P. Quigley, M. Manchester and H. Stuhlmann, *Nat. Med.*, 2006, **12**, 354–360.
- 19 N. F. Steinmetz, A. L. Ablack, J. L. Hickey, B. Manocha, J. s. Mymryk, L. G. Luyt and J. D. Lewis, *Small*, 2011, **7**, 1664–1672.
- 20 N. F. Steinmetz, S. N. Shah, J. E. Barclay, G. Rallapalli, G. P. Lomonosoff and D. J. Evans, *Small*, 2009, **5**, 813–816.
- 21 B. Jung, A. L. Rao and B. Anvari, *ACS Nano*, 2011, **22**, 1243–1252.
- 22 C. Pavlik, N. C. Biswal, F. C. Gaenzler, M. D. Morton, L. T. Kuhn, K. P. Claffey, Q. Zhu and M. B. Smith, *Dyes Pigm.*, 2011, **89**, 1–15.
- 23 H. Gratz, A. Penzkofer, C. Abels, R. M. Szeimies, M. Landthaler and W. Baumler, *J. Photochem. Photobiol., A*, 1999, **128**, 101–109.
- 24 M. L. J. Landsman, G. Kwant, G. A. Mook and W. G. Zijlstra, *J. Appl. Physiol.*, 1976, **40**, 575–583.
- 25 L. V. Wang, *Nat. Photonics*, 2009, **3**, 503–509.
- 26 L. V. Wang and S. Hu, *Science*, 2012, **23**, 1458–1462.
- 27 X. Wang, Y. Pang, G. Ku, G. Stoica and L. V. Wang, *Opt. Lett.*, 2003, **28**, 1739–1741.
- 28 R. I. Siphanto, K. K. Thumma, R. G. Kolkman, T. G. van Leeuwen, F. F. de Mul, J. W. van Neck, L. N. van Adrichem and W. Steenbergen, *Opt. Express*, 2005, **10**, 89–95.
- 29 X. Wang, X. Xie, G. Ku, L. V. Wang and G. Stoica, *J. Biomed. Opt.*, 2008, **11**, 024015.
- 30 R. A. Kruger, W. L. J. Kiser, D. R. Reinecke and G. A. Kruger, *Med. Phys.*, 2003, 856–860.
- 31 H. Fang, K. Maslov and L. V. Wang, *Phys. Rev. Lett.*, 1997, **99**, 184501.
- 32 J. T. Oh, M. L. Li, H. F. Zhang, K. Maslov, G. Stoica and L. V. Wang, *J. Biomed. Opt.*, 2006, **11**, 34032.
- 33 L. V. Wang, *Med. Phys.*, 2008, **35**, 5758–5767.
- 34 C. De Vocht, A. Ranquin, R. Willaert, J. Van Ginderachter, T. Vahnaecke, V. Rogiers, W. Versees, P. Van Gelder and J. Steyaert, *J. Controlled Release*, 2009, **137**, 246–254.
- 35 C. Gabay, *Arthritis Res. Ther.*, 2006, **8**(suppl. 2), S3, DOI: 10.1186/ar1917.
- 36 J. R. Schoenborn and B. C. Wilson, *Adv. Immunol.*, 2007, **96**, 41–101.
- 37 P. Singh, D. Prasuhn, R. M. Yeh, G. Destito, C. S. Rae, K. Osborn, M. G. Finn and M. Manchester, *J. Controlled Release*, 2007, **120**, 41–50.
- 38 C. R. Kaiser, M. L. Flenniken, E. Gillitzer, A. L. Harmsen, A. G. Harmsen, M. A. Jutila, T. Douglas and M. J. Young, *Int. J. Nanomed.*, 2009, **2**, 715–733.
- 39 J. V. Frangioni, *Curr. Opin. Chem. Biol.*, 2003, **7**, 626–634.
- 40 L. T. Hoekstra, W. de Graaf, G. A. Nibourg, M. Heger, R. J. Bennink, B. Stieger and T. M. van Gulik, *Ann. Surg.*, 2013, **257**, 27–36.
- 41 E. Tanaka, F. Y. Chen, R. Flaumenhaft, G. J. Graham, R. G. Laurence and J. V. Frangioni, *J. Thorac. Cardiovasc. Surg.*, 2009, **138**, 133–140.
- 42 S. Yoneya, T. Saito, Y. Komatsu, I. Koyama, K. Takahashi and J. Duvoll-Young, *Invest. Ophthalmol. Visual Sci.*, 1998, **39**, 1286–1290.
- 43 T. Desmettre, J. M. Devoisselle and S. Mordon, *Surv. Ophthalmol.*, 2000, **45**, 15–27.
- 44 P. Ott, S. Keiding, A. H. Johnsen and L. Bass, *Am. J. Physiol.*, 1994, **266**, G1108–G1122.
- 45 V. Saxena, M. Sadoqi and J. Shao, *Int. J. Pharm.*, 2006, **308**, 200–204.
- 46 M. A. Yaseen, J. Yu, M. S. Wong and B. Anvari, *Opt. Express*, 2008, **16**, 20577–20587.
- 47 V. Saxena, M. Sadoqi and J. Shao, *J. Pharm. Sci.*, 2003, **92**, 2090–2097.
- 48 W. Holzer, M. Mauerer, A. Penzkofer, R. M. Szeimies, C. Abels, M. Landthaler and W. Baumler, *J. Photochem. Photobiol., B*, 1998, **47**, 155–164.
- 49 S. Gupta, H. Wilder, A. L. N. Rao, V. I. Vullev and B. Anvari, in *Photonics West: Reporters, Markers, Dyes, Nanoparticles, and Molecular Probes for Biomedical Applications IV*, ed. S. Achilefu and R. Raghavachari, SPIE, San Francisco, CA, 2012, vol. 8233, DOI: 10.1117/1112.907730.